Int J Interact Des Manuf (2016) 10:257–273
DOI 10.1007/s12008-016-0333-4

ORIGINAL PAPER

# Modelling and simulation of direct solar radiation for cost-effectiveness analysis of V-Trough photovoltaic devices

**Andrés Arias–Rosales**[1] · **Ricardo Mejía–Gutiérrez**[1]

Received: 1 June 2016 / Accepted: 15 June 2016 / Published online: 25 June 2016


**Abstract** In the urge to make solar energy competitive enough to directly face fossil fuels, several approaches result crucial for their intended capacity to maximise the energy that can be produced with a given photovoltaic area. Low Concentration Photovoltaics (LCPV) and tracking methods can be integrated in V-Trough solar devices to increase their effective solar harvesting area through low-cost non-imaging optics. As a tool to support the design and simulation of such devices, this work proposes an analytical and numerical model that simulates the interactions of direct solar radiation with the V-Trough's elements. The proposed model is design-oriented and was developed seeking high parameter flexibility, high geometrical detail and low computational demands. The model was experimentally validated through several simulations of V-Trough set-ups which results were compared against measurements with a testing platform. Through a non-parametric statistical analysis, the model proved to be satisfactory and highly accurate. Furthermore, the calculations regarding optical concentration performance were complemented with a cost analysis and integrated into a cost-effectiveness index. The results from this work serve as a useful modelling tool for designing and comparing alternatives of V-Trough solar devices.

**Keywords** Low concentration photovoltaics (LCPV) · Solar V-Trough · Solar tracking · Direct radiation · Geometrical optics · Modelling and simulation

✉ Andrés Arias–Rosales
aariasr@eafit.edu.co

Ricardo Mejía–Gutiérrez
rmejiag@eafit.edu.co

[1] Design Engineering Research Group (GRID), Universidad EAFIT, Cra. 49 N. 7 Sur 50, Medellín, Colombia

## 1 Introduction

In the imperative transit from a fossil fueled civilisation, to a more sustainable and resilient one, solar photovoltaic (PV) energy arises as one of the key energetic approaches that mankind ought to follow [23]. However, solar PV energy is still costly to afford by most of the world's population [2,5] and there is a high level of industrialisation needed to produce solar cells, which could be a considerable limitation for most of the developing countries with the most severe energy needs. Additionally, even though solar PV energy has a comparatively low environmental impact, it still uses some toxic materials and there is not yet the proper infrastructure for large scale recycling of solar panels [17]. Therefore, it is of utmost importance to explore approaches meant to increase the energy production per photovoltaic area in order to reduce the negative effects and seeking to increase the cost-effectiveness through approaches that proportionally cost less.

Several factors limit the energy production performance of regular solar panels. For instance, the effective harvesting area of a common fixed solar panel diminishes with the cosine of the angle of misalignment between the incoming rays and the normal to the panel [33]. On the contrary, a panel with a tracking system follows the apparent movement of the sun on the sky, which reduces the described misalignment, improving the effective harvesting area throughout the day and thus, increasing the daily energy production in up to a 30–50 % [19]. Another way to increase the effective harvesting area is to directly escalate it with non-imaging optic devices, such as lenses [3] and reflective troughs [34]. This approach, known as solar concentration, works by reflecting or refracting the solar rays towards the solar absorber, e.g., a solar cell. Nevertheless, the direction in which the rays are re-directed from the concentrating elements depends on the

angle of incidence of the solar rays, which naturally generates the need to track the sun in order to keep focusing the solar rays into the PV absorber. The higher the level of concentration, the smaller the misalignment that can be tolerated [9]. Therefore, a low concentration method (less than 10 Suns) allows for more flexible possibilities in terms of solar tracking, which the authors consider as an opportunity for design exploration with simple tracking approaches, such as manual tracking [7].

Low concentration photovoltaics (LCPV) can focus sunlight via refraction through lenses, via reflection from mirroring surfaces or via luminescent materials [31]. Correspondingly, several approaches in terms of the optical elements were found and can be mainly classified in either point-focus concentrators, designed for a three-dimensional punctual convergence, or linear-focus, in which the radiation focused is intended to have a constant cross-section and have a two-dimensional linear convergence [2]. The point-focus optics are usually implemented for high concentrations [2], but can also be employed for LCPV mostly with compound parabolic reflectors [2,31] and flat mirror arrays, symmetrical about an axis which is normal to the PV surface [1,31]. The optical elements of linear-focus LCPV consist mainly in Fresnel lenses [10] and reflective troughs of different geometries, i.e., cylindrical, compound parabolic and flat V-Troughs [2]. This work is centred in V-Trough LCPV because of the relative simplicity and low-cost of their optics, i.e., flat mirrors, which results in the potential of a technology that is more affordable, accessible and easier to manufacture and maintain [5,13,14,29,34].

Product design is a complex and holistic endeavour and, in terms of solar devices, it can be better guided with the support of tools that enable the designer to explore the consequences of new product configurations in an insightful and straightforward manner. An ever increasing use of simulation and modelling tools throughout the design process is a clear trend in product design [11,30,36]. In accordance with the so-called Interactive Design, these tools may be used to actively support the designer in the preliminary design phase, allowing for a greater insight into the implications of his/her early decisions [12]. Interactive Design could benefit the design exploration of V-Trough concentrators by enabling the designer to simulate the performance of new ways to concentrate and track the sun and consequently, this could lead to a more cost-effective solar energy production with set-ups beyond the typical configurations.

In order for designers and engineers to take full advantage of the high level of integration and flexibility of combined solar tracking and low concentration with V-Troughs, an appropriate modelling tool is needed that not only delivers a final energy production result, but also that allows for detailed comparisons and explorations and that leads the designers towards a deeper insight into the simulated phenomena. This work describes the development of such a modelling tool, comprising a new mathematical model, which performs a hybrid analytical-numerical 2D geometrical description of the direct radiation's effects on a V-Trough solar device with high flexibility in terms of geometrical and tracking parameters. After the model description, a validation of the analytical core of the model is presented, followed by a proposed cost-effectiveness index and an exploration of the implications of the model with a selection of the simulated V-Trough set-ups used for the validation.

## 2 Literature review

Solar energy is all about harvesting the solar radiation. Therefore, when designing a solar device, it is of great interest to explore how solar radiation reaches the PV absorber and which factors influence its intensity at the PV surface throughout the day. Solar radiation can be described as quantised discrete photons [16] or as a propagating wave [4]. For instance, Penttilä and Lumme [26] used numerical wave-optical methods to simulate light scattering in porous materials. However realistic, these simulations at the level of electromagnetic waves or photons tend to lead to unnecessarily complex and computationally intensive processes when the dimensions of the simulated objects are orders of magnitude greater than the radiation's wavelength of interest [8].

When modelling the solar radiation for concentration and tracking devices, a convenient approach is using geometrical optics, which describes unperturbed sunlight as projected rays which propagate from a given light source in a straight path [8,35]. These rays, as formulated by Pierre de Fermat [35], follow the optical path between two points that can be traversed in the shortest time, taking into account the refractive index of the mediums involved. Since the optical laws derived from Fermat's principle of least time can be described with basic geometry, geometrical optics is considered to be a practical tool for modelling the solar direct rays, so-called beam radiation, since it offers a proper and comprehensive simplification of its macroscopic behaviour.

Beam radiation is not the only solar radiation component to be considered, especially when the simulated application is affected by a non-vacuum medium, such as Earth's atmosphere. Nonetheless, this project focuses entirely on beam radiation because of its major role on concentration and PV energy production in general, which is arguable from the fact that the proportion of direct radiation is commonly taken as 90% of the global radiation as a general approximation [19]. Besides, the deterministic nature of beam radiation allows for its geometrical analysis to turn into comprehensive design insights.

The modelling of beam radiation and its interactions with solar devices can be approximated numerically with Ray trac-

ing algorithms which, in the case of solar direct radiation, are simulated with parallel rays, equally separated, that project themselves from the solar incident direction and interact with the simulated objects by following the laws of geometrical optics. For instance, Bojić et al. [6] modelled sea-shell trough solar concentrators with specular ray tracing methods which focused on beam radiation.

Even though numerical modelling of solar rays may be more flexible and unbiased, analytical models tend to lead to a deeper understanding of the phenomena addressed, which is desirable to gather valuable design insights. Moreover, analytical models tend to be considerably less computationally expensive when it comes to radiation simulation [24,32], and that is a crucial feature for real-time interactive modelling for design purposes. Tina and Scandura [34], Bahaidarah et al. [5], Kostić et al. [20], Reis et al. [27], analytically modelled radiation for V-Trough applications, but with formulations that are over-simplified and not oriented towards a deeper step-by-step geometrical analysis. Fraidenraich [13,14] and Hermenean et al. [18] developed more detailed analytical models of beam radiation for V-Trough solar devices, but the authors of this work believe that a more intuitive and design-oriented analytical model can be developed, going further into the exploration towards design insights, and with a higher flexibility in the selection of geometrical and tracking parameters. Furthermore, it was found that the studied analytical models treated solar tracking and solar concentration separately and considered their effects as additive or took tracking into account only as a miss-alignment factor, as with [13,14,18,34]. Nevertheless, when tracking parameters are given more flexibility, they deeply affect the concentrating effects of the V-Trough optics and hence, both effects should not be treated as additive, but instead as a combined strategy as the proposed model of this work intends to do.

The detailed effects of the combined concentration and tracking strategies over optical performance are crucial for a solar device designer to take decisions but are not enough. The cost implications of these strategies must also be taken into account in order to compare the cost-effectiveness of different design alternatives. Several simple cost-effectiveness analysis were found in literature which take the proportional gain in energy, due to strategies seeking to maximise the output of a PV area, and compare it against the proportional increase in costs, based on area cost estimates [20,22,29,34]. A much more detailed cost-effectiveness analysis was performed by Fraidenraich [14] and is specific for V-Trough PV device, but it is too specifically tied to the beam radiation's model he proposed, which is less flexible than the one proposed in this work. Compared to the approaches found in literature, the authors consider that it is possible to propose a more useful V-Trough cost-effectiveness index, related to a more flexible, comprehensive and insightful model of the beam radiation interactions with the V-trough's elements.

## 3 Proposal of a direct radiation model for V-Trough devices

The objective of this section is to propose a direct radiation model which is intended for designing and comparing alternatives of V-Trough PV devices guided by the simulation of the optical performance. The model was specially designed aiming at future implementations to support the design process of V-Trough devices in a real-time interactive approach; hence the efforts to achieve high parametric flexibility, low computational demands and a detailed and intuitive analysis of the phenomena. Not only was it designed for interactive design purposes, but also it was itself produced through a process aided by interactive design tools. The model was developed in a parallel and systematic approach, where:

- The modelling problem was divided into smaller and simpler optical interaction phenomena, for which corresponding variables were assigned.
- For every variable, an analytical equation was developed through a geometrical assessment of the particular phenomenon being addressed in order to achieve the capacity to predict it.
- By using Microsoft Excel®, the new equation was added to the previous ones and then numerically solved to simulate its behaviour throughout a solar day.
- The numerical data-set was directly inspected in search of mathematical errors and then visualised through line charts developed also in Microsoft Excel®, where a first interpretation of its behaviour took place.
- Several static scenarios where selected from points of interest in the graphs and then further visualised in a more intuitive 3D space by means of a V-Trough simulation developed with the Computer Aided Design Software (CAD) so-called SolidWorks®.
- The Sketch module of SolidWorks® was used to verify the predicted values for the variable being addressed. These verifications were performed by simulating the rays with sketch lines defined to behave according to the laws of geometrical optics.

The described process was carried out until all the defined variables were mathematically described, visualised, verified and added into the main model. Through this systematic approach, aided by the integration of interactive design tools, it was possible to make intuitive sense of every variable being modelled and the geometrical implications and detailed causes of the model's predictions.

In the following subsections, there is an initial conceptual definition, which delimits the addressed phenomena and schematically interrelates the main variables to be calculated in accordance with the direct radiation interactions.

Afterwards, the geometrical construction of the model is described, comprising an analytical core which is then numerically iterated throughout a range of solar elevations $\alpha$, which results in the calculation of the average effective concentration $\overline{C_e}$.

### 3.1 Definition of the conceptual model

This subsection presents the systematic analysis that was developed, based on the principles of geometrical optics, in order to describe the effective optical concentration factor of a given V-Trough set-up related only to beam radiation. The effective optical concentration factor is directly related to the energy that is incident to the PV absorber, coming from beam radiation. The tracking movements are only considered in one axis and therefore, the geometrical analysis can be performed in a two-dimensional simplification assuming total alignment in a third dimension. Accordingly, the model describes the interactions with radiation in terms of lengths, or apertures, perpendicular to the incident sunlight, which are directly proportional to corresponding areas in a third dimension, i.e., depth-wise (see Fig. 3).

This conceptual model considers the main variations in the harvesting area due to the angles of incidence, shadows and reflection losses. In order to simplify the model, without losing considerable accuracy, the model considers up to two consecutive mirror reflections per solar ray, for it was found that more than two bounces is an uncommon phenomenon in V-Trough devices with low concentration factors and do not usually play a considerable role in the total effective suns.

Figure 1 shows the conceptual scheme of the developed proposed model for a certain solar elevation angle $\alpha$. Each V-Trough's element (left mirror, PV area and right mirror) is examined separately for a detailed description. First, the geometric projection of each element is assessed normal to the incident beam radiation, namely the geometrical incidence aperture ($aL_0$, $aPV_0$ and $aR_0$). Then, the direct shadows that each element may cast are calculated ($aL_S$, $aPV_S$ and $aR_S$) and used to find the real incidence aperture of each element ($aL$, $aPV$ and $aR$) by subtracting the blocked rays ($aL_B$, $aPV_B$ and $aR_B$) from the incidence apertures of each element. After the rays directly reach each mirror they will either bounce out of the device, reach the reflective surface of the other mirror, be blocked ($aL_{PVB}$ and $aR_{PVB}$) by the other mirror's casted second shadows ($aR_{LS}$ and $aL_{RS}$) or they may be directly reflected towards the PV area ($aL_{PV}$ and $aR_{PV}$), reduced proportionally to the index of reflection $\rho$ of the mirrors. The rays that reach the other mirror after the first bounce may then either bounce out of the device or reach the PV area after the second bounce ($aL_{RPV}$ and $aR_{LPV}$), in which case they get reduced once again by $\rho$. Afterwards, the effective aperture of the mirrors ($aL_e$ and $aR_e$) can be calculated and, in the case of the PV area, the real incidence aperture $aPV$ is equal to its effective aperture $aPV_e$.

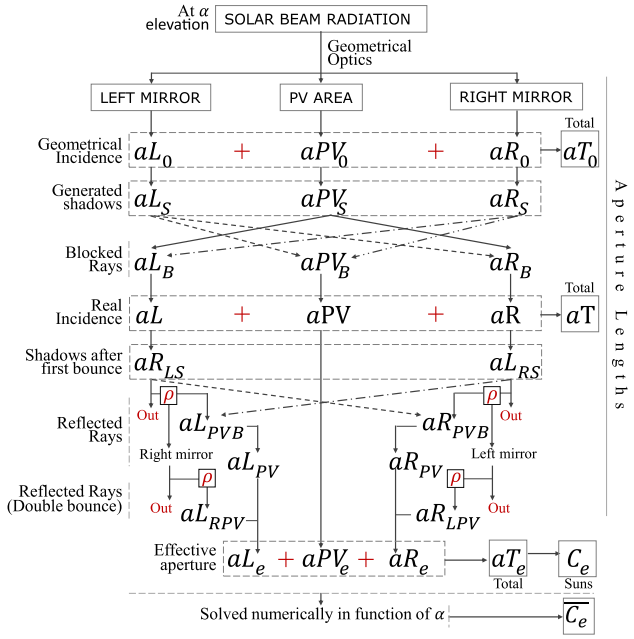


**Fig. 1** Diagram of the conceptual model

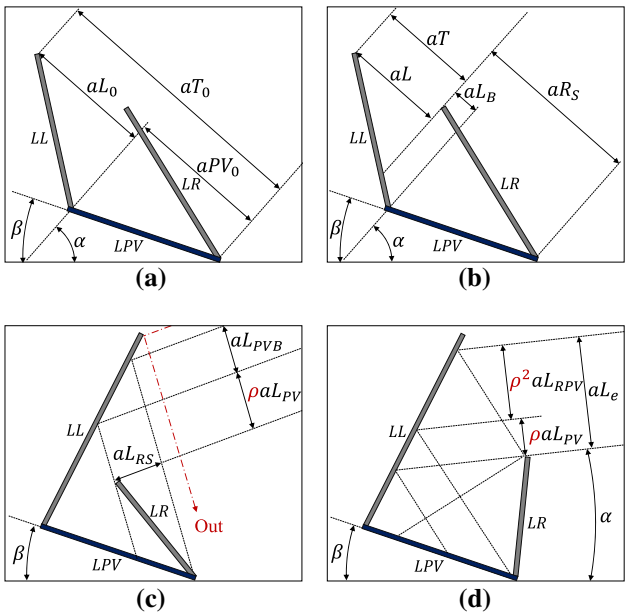


**Fig. 2** Graphical exemplifications of the aperture lengths, normal to the incident rays, analysed by the model

Finally, the effective aperture of the three components conform the total effective aperture $aT_e$, from which the total effective concentration $C_e$ is calculated and iterated numerically in function of $\alpha$ towards an average $\overline{C_e}$.

Figure 2a–d graphically exemplify the variables related in the scheme of Fig. 1. The lengths of the PV absorber, the left mirror and the right mirror are defined by $LPV$, $LL$ and

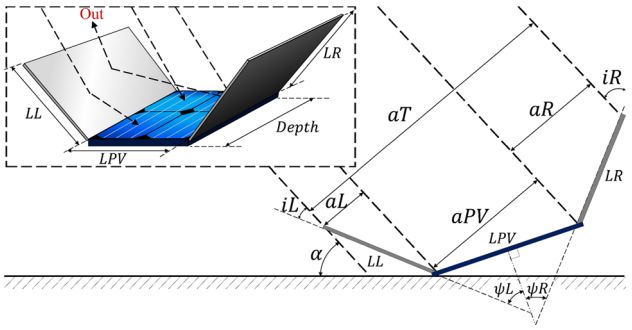


**Fig. 3** 2D & 3D Geometrical diagram of a V-Trough

$LR$, respectively, and the inclination of the PV absorber is defined by $\beta$. Any unit of measurement can be used for the lengths, as long as there is consistency among all the length parameters.

### 3.2 Geometrical construction of the model

The model proposed in this work seeks to offer a deeper insight into the implications of the geometrical parameters of a V-Trough and the solar elevation $\alpha$, over the effective optical concentration $C_e$. The input parameters (see Fig. 3), namely the independent variables that can be deliberately defined by the user, are the lengths of the PV absorber, the left mirror and the right mirror ($LPV$, $LL$ and $LR$), the angular inclinations of the PV absorber and of the mirrors left and right ($\beta$, $\psi L$ and $\psi R$), and the solar elevation $\alpha$; emphasising that for a given static $\alpha$ the model is analytical. In order to simulate the solar apparent movement throughout the day, and any other movement of the V-Trough's elements in function of the solar movement, the model becomes transient and the analytical equations are solved numerically within a given range of $\alpha$. For instance, the PV absorber's inclination $\beta$ can be defined in function of $\alpha$ in order to simulate several tracking methods.

#### *3.2.1 Effective concentration through analytical modelling*

The analytical model was developed by following the conceptual model as shown in Fig. 1. In the definition of the model's equations, absolute values are used as a tool to correctly handle lengths that result negative and conditionals are used to correctly handle boundary conditions.

The first step is to define the angle of incidence between the direct rays and the PV absorber $iPV$, the direct rays and the left mirror $iL$ and between the direct rays and the right mirror $iR$; as described by Eqs. 1, 2 and 3 respectively.

$$iPV = \alpha + \beta \tag{1}$$

$$iL = \psi L - \alpha - \beta + \frac{\pi}{2} \tag{2}$$

$$iR = \psi R + \alpha + \beta - \frac{\pi}{2} \tag{3}$$

Equations 4, 5 and 6 can be used to calculate the aperture of the geometrical incidence for each V-Trough's element, i.e., the PV absorber, the left mirror and the right mirror respectively. The previous results then allow to calculate the aperture of the total geometrical incidence with Eq. 7. It is worth clarifying that these apertures do not take shadows into account yet.

$$aPV_0 = LPV * \sin(iPV) \tag{4}$$

$$aL_0 = LL * \sin(iL) \tag{5}$$

$$aR_0 = LR * \sin(iR) \tag{6}$$

$$aT_0 = \frac{1}{2}(|aPV_0| + |aL_0| + |aR_0| + aPV_0 + aL_0 + aR_0) \tag{7}$$

Considering all the shadows that each element could cast over the other ones, Eqs. 8, 9 and 10 define the aperture length of the real incidence for the three V-trough's elements.

$$aPV = aPV_0 - \frac{1}{2}(|aL_0| + |aR_0| - aL_0 - aR_0) \tag{8}$$

$$aL = aL_0 - \frac{1}{2}\left(\left|aPV_0 - \frac{|aR_0| - aR_0}{2}\right| - aPV_0 + \frac{|aR_0| - aR_0}{2}\right) \tag{9}$$

$$aR = aR_0 - \frac{1}{2}\left(\left|aPV_0 - \frac{|aL_0| - aL_0}{2}\right| - aPV_0 + \frac{|aL_0| - aL_0}{2}\right) \tag{10}$$

The aperture of the total real incidence $aT$, which represents the rays reaching the V-Trough's reflective surfaces or the PV absorber, is defined by Eq. 11.

$$aT = \frac{1}{2}(|aPV| + |aL| + |aR| + aPV + aL + aR) \tag{11}$$

The incident optical concentration $C$ is defined by Eq. 12. The variable $C$ relates to the proportion of beam radiation that reaches the device as a whole, regardless of whether the radiation reaches the PV absorber or not.

$$C = \frac{aT}{LPV} \tag{12}$$

In order to assess the possible scenarios after the rays are reflected from the mirrors, it is necessary to calculate the angle of incidence of the rays after being reflected once, relative to the mirrors left and right ($iL_R$ and $iR_L$) and relative to the PV absorber arriving from the mirrors left and right

($iL_{PV}$ and $iR_{PV}$); which are defined by Eqs. 13–16 respectively.

$$iL_R = \psi R + 2\psi L - \alpha - \beta + \frac{\pi}{2} \tag{13}$$

$$iR_L = \psi L + 2\psi R + \alpha + \beta - \frac{\pi}{2} \tag{14}$$

$$iL_{PV} = -2\psi L + \alpha + \beta \tag{15}$$

$$iR_{PV} = \pi - 2\psi R - \alpha - \beta \tag{16}$$

After the rays go through their first bounce in certain configurations, as seen in Fig. 2(c), they may be blocked by the shadow casted from the back part of the opposing mirror ($aR_{LS}$ and $aL_{RS}$) which can be calculated with Eqs. 17 and 18. For instance, $aR_{LS}$ defines the aperture length of the shadow casted by the left mirror regarding the rays which were reflected from the right mirror and may keep them, completely or partially, from reaching the PV absorber.

$$aR_{LS} = LL * \sin(iR_L) \tag{17}$$

$$aL_{RS} = LR * \sin(iL_R) \tag{18}$$

The following step, described by Eqs. 19 and 20, consists in calculating the allowable aperture lengths of each mirror ($p_L$ and $p_R$) such that, if rays reach them with relative incidences ($iL$ and $iR$), rays would be focused towards the PV absorber, taking into account the calculated second shadows ($aR_{LS}$ and $aL_{RS}$) .

$$p_L = LPV * \sin(iL_{PV}) - \frac{|aL_{RS}| - aL_{RS}}{2} \tag{19}$$

$$p_R = LPV * \sin(iR_{PV}) - \frac{|aR_{LS}| - aR_{LS}}{2} \tag{20}$$

Several special boundary cases were found when relating $aL_0$, $aR_0$, $aL$, $aR$, $p_L$ and $p_R$ in order to find the apertures which describe the rays directly reflected towards the PV area after only one reflection from the mirrors left or right ($aL_{PV}$ or $aR_{PV}$ respectively). Figure 4 illustrates the most interesting cases, exemplified with the left mirror, highlighting the objective aperture with a grey area in the background.

Figure 4a presents the case where the allowable aperture is greater than the geometrical incidence, in which case all the rays described by the real incidence may reach the PV absorber directly afterwards. Figure 4b illustrates the case where the allowable aperture is somewhere in between the boundaries of the real incidence aperture. Figure 4c corresponds to the case where there is no overlap between the allowable aperture and the real incidence aperture, in which case none of the rays that get reflected from the left mirror, in a first bounce, are expected to reach the PV absorber.

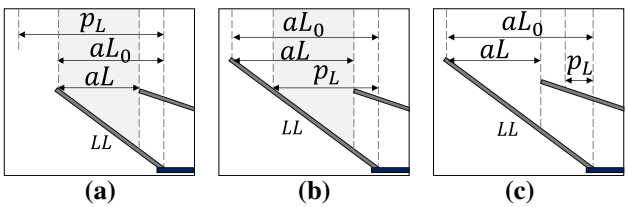


**Fig. 4** Special boundary cases to consider when defining $aL_{PV}$

The angle of incidence between the PV absorber and the rays reflected for the first time from each mirror must also be taken into account. When these angles, $iL_{PV}$ and $iR_{PV}$ described by Eqs. 15 and 16, are $\leq 0$ it means that the firstly reflected rays will not intercept the PV in their direction of advance. The previous fact, as well as the boundary cases shown in Fig. 4, are considered in Eqs. 21 and 22, defining $aL_{PV}$ and $aR_{PV}$ respectively.

$$\begin{aligned} aL_{PV} &= \frac{(|aL_0 - p_L| - 2aL + aL_0 - p_L)}{4\,(aL_0 - p_L - aL)} \\ &\quad * (|aL_0 - p_L - aL| - aL_0 + p_L + aL) \\ &= \begin{cases} 0, & \text{if } iL_{PV} \leq 0 \\ 0, & \text{if } aL_0 \leq 0 \\ 0, & \text{if } (aL_0 - p_L - aL) = 0 \end{cases} \end{aligned} \tag{21}$$

$$\begin{aligned} aR_{PV} &= \frac{(|aR_0 - p_R| - 2aR + aR_0 - p_R)}{4\,(aR_0 - p_R - aR)} \\ &\quad * (|aR_0 - p_R - aR| - aR_0 + p_R + aR) \\ &= \begin{cases} 0, & \text{if } iR_{PV} \leq 0 \\ 0, & \text{if } aR_0 \leq 0 \\ 0, & \text{if } (aR_0 - p_R - aR) = 0 \end{cases} \end{aligned} \tag{22}$$

Figure 5 presents a diagram of a representative situation where certain rays reach the PV absorber after bouncing off the left mirror and then off the right one, described by $aL_{RPV}$. Similarly as with the angles of incidence $iL_{PV}$ and $iR_{PV}$, $iL_{RPV}$ and $iR_{LPV}$ follow the same concept but for the second bounce of the rays (see Fig. 5). The aperture $m_{LR}$ represents the proportion of rays that can access the reflective surface of the left mirror and that may be reflected towards the right mirror when $aL_{PV}$ is subtracted from it; $p_{LR}$ is a similar concept to $p_L$ but applied for the second bounce; $f_{LR}$ represents the left mirror's length projected normal to the rays of the first bounce; and $aL_{RS}$ is used here as the right mirror's length projected normal to the rays of the first bounce. The new previously described variables are defined, for both mirrors, by Eqs. 23–32.

$$iL_{RPV} = -2\psi L - 2\psi R + \alpha + \beta \tag{23}$$

$$iR_{LPV} = \pi - 2\psi R - 2\psi L - \alpha - \beta \tag{24}$$

$$m_{LR} = aL - aL_{PV} \tag{25}$$

$$m_{RL} = aR - aR_{PV} \tag{26}$$

$$p_{LR} = LPV * \sin(iL_{RPV}) \tag{27}$$

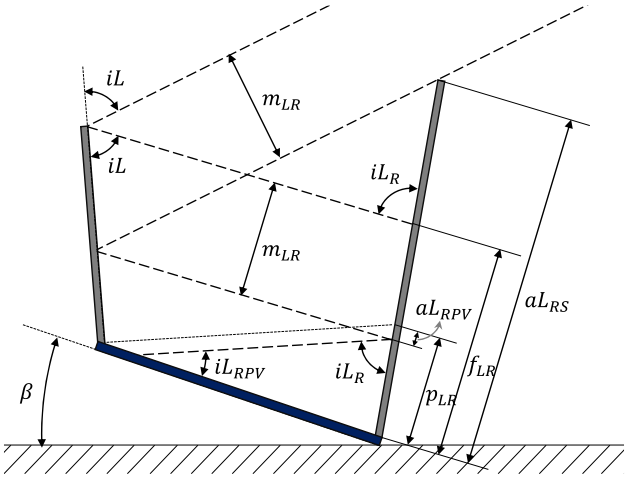


**Fig. 5** Diagram of a case where certain rays reach the PV absorber after two bounces

$$p_{RL} = LPV * \sin(iR_{LPV}) \tag{28}$$

$$f_{LR} = D_{LR} * \sin\left(iL - \arcsin\left(\frac{LPV * \cos(\psi L)}{D_{LR}}\right)\right) \tag{29}$$

$$f_{RL} = D_{RL} * \sin\left(iR - \arcsin\left(\frac{LPV * \cos(\psi R)}{D_{RL}}\right)\right) \tag{30}$$

Where

$$D_{LR} = \sqrt{LL^2 + LPV^2 + LL * LPV * 2\sin(\psi L)} \tag{31}$$

$$D_{RL} = \sqrt{LR^2 + LPV^2 + LR * LPV * 2\sin(\psi R)} \tag{32}$$

Similarly as with the Fig. 4, the diagrams of Fig. 6 illustrate the most interesting boundary cases to consider in order to properly define the aperture of the rays that reach the PV absorber after a second bounce, exemplified in the figure with the rays that first bounce off the left mirror and then off the right one. The aperture of interest for the example, $aL_{RPV}$, is represented in the figure with a greyed area.

Figure 6a, e show cases in which the aperture of interest is limited in the upper boundary by the allowable aperture $p_{LR}$, while in Fig. 6d, f the upper boundary is defined by the aperture relative to the right mirror's length $aL_{RS}$ for the second bounce. In the case of Fig. 6b, c, the variable $aL_{RS} = 0$ because either $p_{LR}$ or $aL_{RS}$ is too small to overlap with $m_{LR}$. Figure 6g represents the case where all the rays that do reach the right mirror, after bouncing off the left one, will reach the PV absorber.

From the analysed geometrical cases, it was found that $aL_{RPV}$ and $aR_{LPV}$ must fall inside the apertures described by $m_{LR}$ and $m_{RL}$ and can be reduced according to the minimum value among $[aL_{RS}, f_{LR}, p_{LR}]$ and, for the right side case, the minimum value among $[aR_{LS}, f_{RL}, p_{RL}]$. Equations 33 and 34 define the corresponding aperture lengths of the rays that reach the PV absorber after bouncing off both mirrors, starting by the left mirror $aL_{RPV}$ and by the right mirror $aR_{LPV}$.

$$\begin{aligned} aL_{RPV} &= \frac{1}{2}\left(|m_{LR} - f_{LR} + min[aL_{RS}, f_{LR}, p_{LR}]| \right. \\ &\quad \left. + m_{LR} - f_{LR} + min[aL_{RS}, f_{LR}, p_{LR}]\right) \\ &= \begin{cases} 0, & \text{if } iL_{RPV} \le 0 \\ 0, & \text{if } m_{LR} = 0 \\ 0, & \text{if } p_L \ge aL_0 \end{cases} \end{aligned} \tag{33}$$

$$\begin{aligned} aR_{LPV} &= \frac{1}{2}\left(|m_{RL} - f_{RL} + min[aR_{LS}, f_{RL}, p_{RL}]| \right. \\ &\quad \left. + m_{RL} - f_{RL} + min[aR_{LS}, f_{RL}, p_{RL}]\right) \\ &= \begin{cases} 0, & \text{if } iR_{LPV} \le 0 \\ 0, & \text{if } m_{RL} = 0 \\ 0, & \text{if } p_R \ge aR_0 \end{cases} \end{aligned} \tag{34}$$

Subsequently, the effective apertures of the three elements of a V-Trough can be calculated with Eqs. 35–37.

$$aPV_e = \frac{|aPV| + aPV}{2} \tag{35}$$

$$aL_e = \rho * aL_{PV} + \rho^2 * aL_{RPV} \tag{36}$$

$$aR_e = \rho * aR_{PV} + \rho^2 * aR_{LPV} \tag{37}$$

Afterwards, the resulting effective concentration can be calculated with Eq. 38.

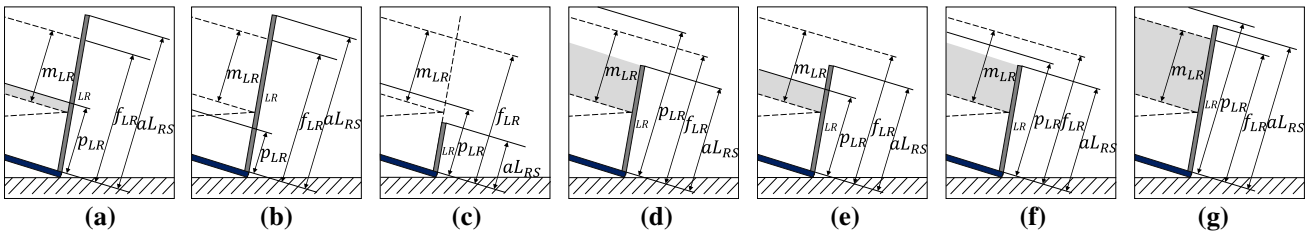


**Fig. 6** Special boundary cases to consider when defining $aL_{RPV}$

$$C_e = \frac{aPV_e + aL_e + aR_e}{LPV} \tag{38}$$

The effective optical concentration $C_e$ is thus a variable solved analytically for a given static $\alpha$. $C_e$ is a dimensionless index, since it is defined as proportional to the length of the PV absorber, and can be interpreted as the number of effective optical concentrating suns in terms of the energy incident to the PV absorber for a given $\alpha$. As a reference for comparison, a solar cell without concentrating mirrors, and placed perpendicular to the incident direct rays, would result in $C_e = 1$ proportional suns of beam radiation.

#### 3.2.2 Average effective concentration through numerical modelling

As it was indicated in Fig. 1, $C_e$ can be solved numerically, with Eq. 39, for a range of $\alpha$ solar elevations and averaged in order to get $\overline{C_e}$, which represents the optical performance of a V-Trough solar device for a given range of time.

$$\overline{C_e} = \frac{\sum_{i=0}^{\left[\frac{\alpha_c - \alpha_f}{\alpha_s}\right]} C_{e(\alpha_f + i*\alpha_s)}}{\frac{\alpha_c - \alpha_f}{\alpha_s} + 1} \tag{39}$$

With $\alpha_f$ = The "floor" or lowest value for $\alpha$, $\alpha_c$ = the "ceiling" or greatest value for $\alpha$ and $\alpha_s$ = the angular step value between the wanted $\alpha$ values.

In Eq. 39 $C_e$ is defined in function of the solar elevation $\alpha$ according to the limits and the step of the range values. The Expression 40 shows that $C_e$ is in fact in function of $\alpha$ and the geometrical parameters of the V-Trough, i.e., the angular inclinations of the PV absorber and of the mirrors left and right ($\beta$, $\psi L$ and $\psi R$) and the lengths of the PV absorber and the two mirrors ($LPV$, $LL$ and $LR$). The Expression 40 represents V-Trough set-ups in which the geometrical parameters of the device are left static but the solar elevation is considered as a dynamic variable that conditions the effective optical concentration. On the other hand, the Expression 41 states $C_e$ as a function of the same parameters as in Expression 40 but they are themselves in function of the solar elevation, which represents a V-Trough device set-up in which any of its geometrical parameters can have a solar tracking dynamic response. The user can deliberately define any of those parameters to be static or dynamic and, in the latter case, the user may define any function relating the parameters to the solar elevation, as long as the resulting input values respect the ranges presented in Table 1.

$$C_{e(\alpha,\beta,\psi L,\psi R,LPV,LL,LR,\rho)} \tag{40}$$

$$C_{e(\alpha,\beta_{(\alpha)},\psi L_{(\alpha)},\psi R_{(\alpha)},LPV_{(\alpha)},LL_{(\alpha)},LR_{(\alpha)},\rho_{(\alpha)})} \tag{41}$$

**Table 1** Minimum and maximum values allowable for the input parameters

| | $\alpha$ | $\beta$ | $\psi L$ | $\psi R$ | $LPV$ | $LL$ | $LR$ | $\rho$ |
|---|---|---|---|---|---|---|---|---|
| Min | 0 | $-\pi$ | $-\pi/2$ | $-\pi/2$ | 0 | 0 | 0 | 0 |
| Max | $\pi$ | $\pi$ | $\pi/2$ | $\pi/2$ | $\infty$ | $\infty$ | $\infty$ | 1 |

## 4 Validation of the proposed direct radiation model

The proposed model calculates the effective optical concentration due to beam radiation, which relates to the beam radiation's energy that would reach a PV absorber in a V-Trough device. However, the outputs from the model are not yet directly defining the electric output of the PV device, since the model does not consider neither thermal losses, nor electrical losses in the semiconductor, nor the interactions with diffuse radiation. Before complementing the proposed model in further work, by considering such losses and other solar radiation's elements, it is crucial to validate its capacity to accurately account for the effective optical concentrating factor of beam radiation in a V-Trough PV device. Correspondingly, laser devices may be used to experimentally model and corroborate specific predictions about the solar beam radiation's behaviour, since laser beams, for practical matters at this scale, follow the basic principles of geometrical optics in the same way as beam radiation [25].

An experiment was designed with the objective to validate the proposed direct radiation model through laser measurements. Part of the aim of the experiment is to directly analyse the optical events of the simulated phenomena, challenging the systematic description performed in the conceptual model and the mathematical formulations of the model itself. In order to perform the experiment, a testing platform was developed to carry out the measurements and to adopt the geometries and movements of a V-Trough device. Subsequently, the experimental results are statistically compared to the model's predictions and the interpretations of the results are then presented.

### 4.1 Design of the experiment

The proposed direct radiation model calculates and relates a series of proportional lengths in order to produce a final concept of effective optical concentration. The central concept of the experiment is that these calculated lengths, dependant of a given set of geometrical input parameters, are specific predictions that can be compared against real laser measurements of those same lengths. Those experimental measurements were defined to be performed in a testing platform capable of adopting the same geometries as the ones in the simulations. If the model is correctly defined, it is expected that the predicted values would not vary significantly from the

**Table 2** Input parameters of the simulated V-Trough set-ups. Those designed with D and those randomly defined with S

| Set-Up | $LPV$ | $LL$ | $LR$ | $\psi L$ | $\psi R$ | $\beta_i$ | $\beta_{\alpha s}$ | $\beta_s$ |
|---|---|---|---|---|---|---|---|---|
| D1 | 1 | 1 | 1 | $2\pi/15$ | $2\pi/15$ | $\pi/3$ | $\pi/3$ | $-\pi/3$ |
| D2 | 1 | 1 | 1 | $\psi L_{(\alpha)}$ | $\psi R_{(\alpha)}$ | $\pi/4$ | $\pi/2$ | $-\pi/2$ |
| D3 | 1 | 1 | 1 | $\psi L_{(\alpha)}$ | $\psi R_{(\alpha)}$ | 0 | 0 | 0 |
| D4 | 1 | $LL_{(\alpha)}$ | $LR_{(\alpha)}$ | 0 | 0 | 0 | 0 | 0 |
| D5 | 1 | 1.5 | 0.5 | $\psi L_{(\alpha)}$ | $\psi R_{(\alpha)}$ | $\pi/4$ | $\pi/2$ | $-\pi/2$ |
| S1 | 1 | 0.9 | 1.35 | $-6\pi/23$ | $5\pi/36$ | $\pi/14$ | $3\pi/20$ | $-14\pi/29$ |
| S2 | 1 | 0.4 | 0.7 | $-\pi/35$ | $5\pi/22$ | $2\pi/9$ | $\pi/12$ | $-36\pi/41$ |
| S3 | 1 | 0.65 | 0.95 | $-5\pi/31$ | $36\pi/79$ | $\pi/3$ | $\pi/26$ | $-9\pi/29$ |
| S4 | 1 | 0.85 | 0.7 | $-\pi/90$ | $3\pi/11$ | $14\pi/37$ | $\pi/35$ | $-13\pi/14$ |
| S5 | 1 | 1 | 1.3 | $\pi/90$ | $13\pi/33$ | $11\pi/46$ | $45\pi/89$ | $-2\pi/17$ |
| S6 | 1 | 0.65 | 1.45 | $3\pi/20$ | $\pi/14$ | $-13\pi/33$ | $2\pi/21$ | $-5\pi/23$ |

measured values as long as the geometrical input parameters respect the allowable ranges of Table 1.

The dependant response variable is continuous and defined by proportional lengths, which can be calculated by the equations that conform the proposed model and vary in function of the combination of geometrical inputs, namely $\alpha$, $\beta$, $\psi L$, $\psi R$, $LPV$, $LL$ and $LR$. The index of reflection $\rho$ does not affect the aperture lengths being compared in the experiment and therefore, it is taken as $\rho = 1$. There were 11 V-Trough set-ups defined and, for every set-up, there were four $\alpha$ values selected to perform aperture length calculations and the corresponding measurements. Furthermore, for every $\alpha$, the aperture lengths that were considered were $aPV_e$, $aL$, $aR$, $aL_{PV}$, $aR_{PV}$, $aL_{RPV}$ and $aR_{LPV}$. Therefore, there were 308 length predictions, which were correspondingly compared against 308 experimental measurements.

All the V-Trough set-ups were defined with a dynamic $\beta$ function in order to simulate solar tracking. The $\beta$ function is hence defined by Expression 42, where $\left\lfloor \frac{\alpha}{\beta_{\alpha s}} \right\rfloor$ means that the expression inside must be rounded down.

$$\beta_{(\alpha,\beta_i,\beta_{\alpha s},\beta_s)} = \beta_i + \beta_s * \left\lfloor \frac{\alpha}{\beta_{\alpha s}} \right\rfloor \tag{42}$$

With $\beta_i$ = Initial $\beta$ inclination, $\beta_{\alpha s}$ = Step variation of $\alpha$ needed for every variation in $\beta$ and $\beta_s$ = Step variation of $\beta$ every tracking movement. Accordingly, $\beta$ starts at $\beta_i$ and it varies $\beta_s$ every $\beta_{\alpha s}$ variation of $\alpha$. However, even if the parameters that define $\beta$ are within the allowable ranges, $\beta$ itself may result outside $[-\pi, \pi]$, which could lead to inaccurate calculations from the model. This is a situation that may easily arise when defining any of the input angular parameters as dynamic, but may as easily be corrected by entering equivalent angles which do respect the allowable ranges.

From the 11 defined set-ups, 6 were defined by an algorithm that randomly selected values for every input parameter within the allowable ranges. The parameters were defined randomly to avoid possible bias and with the expectation that more unconventional and unintuitive set-ups could be more challenging for the predictions of a systematically developed model. The other 5 set-ups were deliberately designed by the authors in order to address more realistic and representative V-Trough strategies. Among those 5 set-ups, some were defined with other dynamic parameters in function of solar elevation, besides $\beta$, such as with the individual lengths and inclinations of the mirrors. Since the lengths are analysed as proportional to the PV absorber's length, the latter was defined for all the set-ups as $LPV = 1$. Also, for the sake of practicality in experimental measurements, the lengths of the mirrors were limited to maximum $LL = LR = 1.5 * LPV$. A summary table of the set-up parameters is presented in Table 2, with the lengths given as dimensionless proportions of the PV length, the angles given in radians and the dynamically defined parameters shown as in function of $\alpha$.

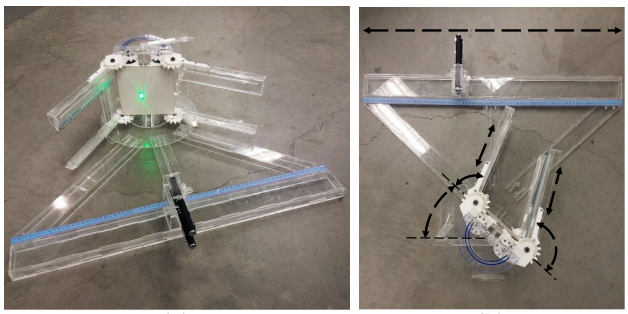

**(a)** **(b)**

**Fig. 7** Testing platform for the validation of the model

In order to validate the previously described 308 predictions related to the 11 defined V-Trough set-ups, a testing platform was developed. Figure 7a shows the platform, which is capable of accurately adopting all the geometries needed to test the 11 set-ups and explore in detail the interactions between beam radiation and the V-Trough's elements via lasers. Through the degrees of freedom, shown with arrows in

Fig. 7b, it is also possible to experimentally simulate different solar elevations $\alpha$ by controlling the angular orientation of the laser beams incident to the device.

The testing process consists in first adopting a particular geometrical configuration of the platform in accordance to one of the set-up's parameters and to the current $\alpha$ to simulate. Afterwards, the aperture lengths $aPV_e$, $aL$, $aR$, $aL_{PV}$, $aR_{PV}$, $aL_{RPV}$ and $aR_{LPV}$ are directly measured by sliding the lasers and detecting starting and ending events. The distance between those events defines the measured lengths. For instance, if the current aim is to measure $aL_{PV}$, it is possible to slide the laser and detect when the laser beam starts reaching the PV absorber after one bounce off the left mirror and then keep sliding it until the phenomenon ceases to occur.

### 4.2 Experiment results and statistical analysis

The original data was defined as aperture lengths and then transformed for the statistical analysis into proportions of the PV absorber's length, which is directly proportional to the PV area as well. The results of the experiment were analysed through a linear regression of the measured values in function of the model predictions. The points of the regression are in fact coordinates from the couples of model predictions with the corresponding experimental measurements. If the predictions relate well to the real measurements, the expected result of the regression would be a straight line with slope tending to 1 and $y$ intercept tending to 0.

Figure 8 graphically shows the performed regression and the calculated equation of the regression line, with a highly satisfactory slope of 0.9931 and a $y$ intercept of 0.0007. The coefficient of determination $R^2 = 0.9977$ resulted considerably high, implying that 99.77 % of the variance of the measurement values is predictable from the variation of the independent variable, i.e., the model predictions.

The residual standard deviation, so-called Standard error of estimate, was calculated to be $SE = 0.0157$, which can be interpreted as the 1.57 % of the PV area. Figure 8 also shows the 95 % Prediction Interval, which defines a range within which a new response in the Measurements variable is 95% likely to fall given a specified value in the Model Predictions variable. This prediction interval can be used to estimate the expected accuracy for future predicted aperture lengths from the model and the method implemented to define this interval is specified later in this section.

To test the significance of the regression, a parametric test was performed, which results are summarised in Table 3. According to the shown $P$-value, the regression is by convention extremely statistically significant, which means that it is extremely unlikely that randomness alone could have been the causal reason for the observed linear behaviour. Therefore, the null hypothesis of random causality is rejected and, in terms of regression, it is thus accepted that the variable

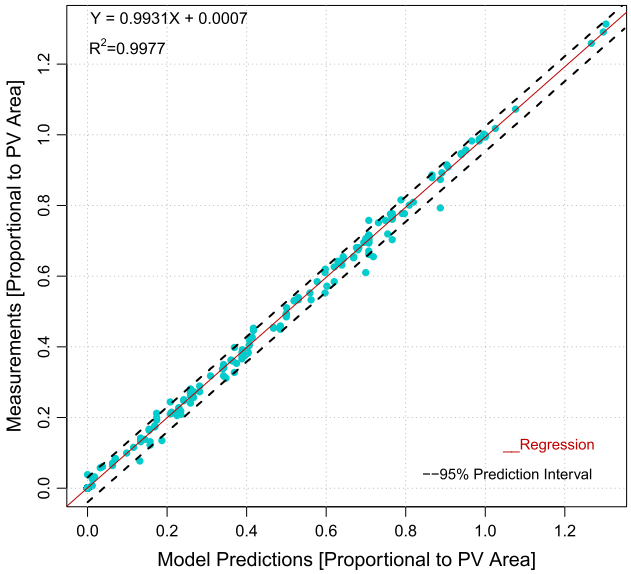


**Fig. 8** Graph of the regression model

**Table 3** ANOVA table of the regression model

| Source | *DF* | *SS* | *MS* | *F*-value | *P*-value |
|---|---|---|---|---|---|
| Regression | 1 | 33.29 | 33.29 | 135512 | $<2e-16$ ** |
| Residuals | 306 | 0.08 | 0.00025 | | |

Model Predictions is of use in explaining the variability in the variable Measurements.

In order to be confident on the results shown in Table 3, it is necessary to analyse the parametric assumptions related to the residuals, i.e., normality and homoscedasticity. Figure 9a shows the scatter-plot of the standardised residuals and 9b presents a histogram of the residuals. There is not an evident or systematic pattern within the residuals, which implies that the regression model fits the data properly. However, it is evident from the histogram that the residuals are not normally distributed, tending more towards zero in a so-called state of thin-tails distribution. The appreciation about non-normality was corroborated with Shapiro-Wilk and Anderson-Darling normality tests, which resulted significant with $P$-values $< 2.2e-16$ for both tests. Several transformations of the data were implemented, namely $(1/y)$, $ln\,(y+1)$, $log_{10}\,(y+1)$, $\sqrt{y}$ and arcsin; but none of the transformations could satisfy the parametric assumptions for the residuals.

According to Reis et al. "thin-tail violations of normality are generally benign" [28]. However, significant violations of normality may affect the validity and precision of inferences made from parametric tests of statistical hypothesis, confidence intervals and prediction intervals. Therefore, it was defined to analyse the results via non-parametric methods, i.e., Monte Carlo randomisation hypothesis test and

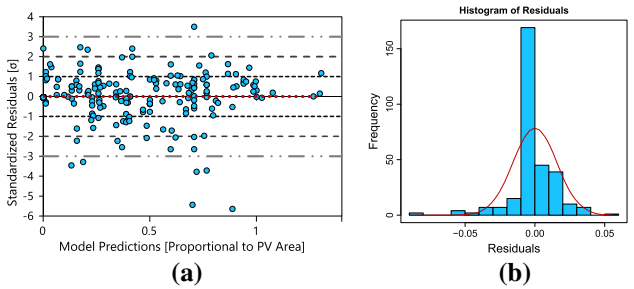


**Fig. 9** Analysis of the regression residuals

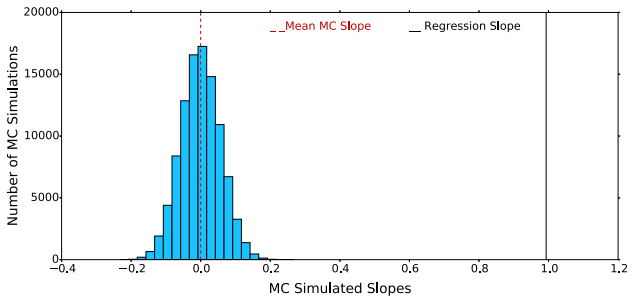


**Fig. 10** Monte Carlo test of hypothesis

Bootstrapping intervals, and to later compare them with the previous parametric results shown in Table 3.

A non-parametric method, so-called Monte Carlo randomisation, was implemented to test hypotheses regarding the slope of the regression, as indicated by [15]. After 100,000 Monte Carlo simulations, the number of times that a randomly simulated regression slope was equal or greater than the observed slope of the model was 0. The previous result implies, in accordance with the parametric results, that the regression is extremely statistically significant with a $P$-value tending to 0. Figure 10 illustrates the Monte Carlo method implemented, where a histogram is shown of the simulated slopes calculated from every reshuffling of the data. From this figure it is evident that the randomness effect is far from reaching the slope obtained by the original regression.

Even though the significance of the regression is now evident, it is also of great interest to test if the slope of the regression is statistically equivalent to 1, which is the value expected from an ideal correspondence between a model's predictions and the respective measurements. To test this hypothesis, it is necessary to analyse if the effect of randomness could have been the major cause of the delta between the slope of the regression model and an ideal slope of 1, which resulted in $\Delta m = 0.0068$. Within the Monte Carlo simulations, 90324 was the number of times that a simulated slope attained an equal or greater absolute delta from their mean slope, as compared to $\Delta m$ of the regression. Therefore, the significance level for the regression's $\Delta m$, from a slope 1, corresponds to a high P-value = 0.90324. From the previous result, it can be deduced that the slope achieved by the regression model is statistically equivalent to 1, since it is very likely that the delta from 1 could have been caused mainly by randomness.

It is also of interest to test a similar hypothesis for the $y$ intercept to assess its delta from 0; $\Delta I$. It was found that the significance level for the regression's $\Delta I$, from a $y$ intercept of 0, corresponds to the $P$-value = 0.96171. As with the slope, from the previous result it can be inferred that the $y$ intercept of the regression model is statistically equivalent to 0. Consequently, it can be assumed that the regression model as a whole, is statistically equivalent to the ideal expected model, where $Y = X$.

Considering that the regression proposes the linear model for a population of data, but based only on a sample, confidence intervals are a useful way of estimating the likely ranges for the real linear parameters of the whole population of possible data. Since residuals cannot be assumed to be normally distributed, a non-parametric method, so-called Bootstrapping [21], can be used to estimate such intervals as well as prediction intervals. In fact, the 95 % Prediction Interval for the estimated response variable, shown in Fig. 8, was calculated through this method. The average ceiling for this prediction interval was 0.03 higher than the estimated response variable and the average floor of the interval was 0.041 below the estimated response variable. The previous means that, if the current regression model is applied to new data, it is expected that 95 % of the times the real values would fall in an interval than would at maximum underestimate the PV area in a 3 % or overestimate it in a 4.1 %.

Through Bootstrapping it was also possible to calculate that the real slope of the data is 95 % likely to be between [0.987, 0.999] and similarly, that the real $y$ intercept is 95 % likely to be between $[-0.00065, 0.00216]$. Those narrow confidence intervals imply favourable expectations in terms of the accuracy of the regression model, since even the boundaries of those intervals are still virtually identical to the ideal values. Figure 11 shows the frequency distribution of the Bootstrapping slopes with 11(a) and $y$ intercepts with 11(b). For the distribution of every statistic calculated, 100000 Bootstrapping reshuffling simulations were performed.

To analyse the implications of the accuracy of the validated model over the most important resulting calculations, i.e., incident optical concentration $C$ and effective optical concentration $C_e$, a comparison was made between those variables calculated from the model predictions against the same variables but calculated directly from the experimental measurements. On average, the model predictions resulted in a $C$ that is 0.56 % less than the experimentally measured value and in a $C_e$ that is on average 0.31 % greater than the experimentally measured value.

Figure 12 presents, for all the tested V-trough set-ups, the percentage errors between modelled and measured $C$, with $EC$, and between modelled and measured $C_e$ with $EC_e$. The

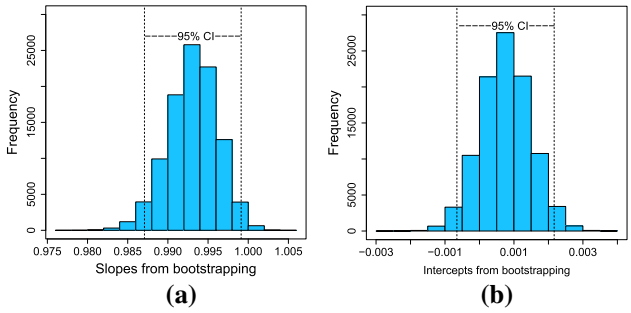


**Fig. 11** Bootstrapping confidence intervals for the slope and the $y$ intercept

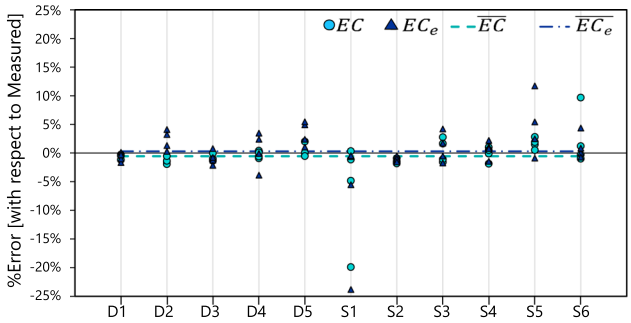


**Fig. 12** Percentage error between predicted and measured incident and effective optical concentration

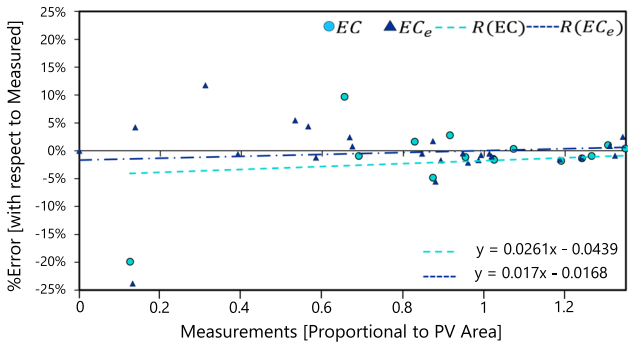


**Fig. 13** Percentage error between predicted and measured incident and effective optical concentration, in function of the Measurements

figure also shows the average percentage errors with $\overline{EC_e}$ and $\overline{EC}$.

Figure 13 explores the behaviour of $EC$ and $EC_e$ plotted against the Measurements proportional to the PV area. Two linear regressions were performed, for $EC$ with $R\,(EC)$ and for $EC_e$ with $R\,(EC_e)$, which lines and equations are also shown in the figure. Both regressions show a tendency towards higher proportional errors towards the smallest Measurements. This tendency makes intuitive sense because, if the errors in aperture lengths behave altogether as homogeneous with random variations, they would be expected to cause a smaller impact when affecting proportionally greater Measurements, and vice versa.

Considering the results of the statistical analysis, in particular the behaviour of the residuals, it is reasonable to support the hypothesis that most of the errors between the model's predictions and the measurements, however small, correspond to random errors in the measurement process, either due to the precision in detecting the optical events or due to structural imprecision in the testing platform. Even so, the results are statistically equivalent to the ideally expected behaviour and the proposed geometrical model is considered to have been satisfactorily corroborated.

## 5 Cost-effectiveness analysis

With the described analytical-numerical model, it is possible to calculate the average effective optical concentration $\overline{C_e}$, which is of great use to compare V-Trough alternatives with equivalent mirror area. However, when comparing alternatives with considerable differences in the proportion of the mirrors, $\overline{C_e}$ alone may lead to misleading design decisions. For instance, an alternative may be able to double the $\overline{C_e}$ of a PV absorber, but if it does so by triplicating the cost of the device due to considerably big mirrors, then the implementation of a V-Trough such as that one would not be cost-effective.

Consequently, it is the intention of the authors to propose a useful cost-effectiveness index $I_{COE}$ for comparing V-Trough PV devices by contrasting the gain of incident energy, due to the resulting $\overline{C_e}$ , against the added cost due to the mirrors and extra supporting structure. It is worth noting that it is not the intention of this work to offer an all-encompassing index to take final decisions of cost-effectiveness, since that would imply taking into account the interactions with diffuse radiation and the losses due to temperature and non-uniform illumination, among others. Moreover, the proposed index does not take into account the tracking costs, since it focuses on manual tracking and other simple tracking actuation methods, such as water dripping. However, the index of this work may be useful to make broad first comparisons within the limitations of the model proposed and may be complemented with other factors in further work.

In order for the index $I_{COE}$ to be more intuitive, it is defined in proportion of a reference set-up, which consists in a fixed PV absorber with no concentrating mirrors. This way, if $I_{COE} > 1$, it may imply that the alternative being assessed has a better cost-effectiveness than the reference. Conversely, if $I_{COE} < 1$, it may imply that it is not worth employing the V-Trough set-up being analysed, since it probably would perform worse than a simpler fixed PV absorber with no mirrors.

Equation 43 defines the proposed cost-effectiveness index and specifies that it is in function of a given range of solar elevations, going from a floor $\alpha_f$ to an angular ceiling of $\alpha_c$.

Accordingly, $\overline{C_e}$ and $\overline{C_{eRef}}$ are also stated in function of the same solar elevation range, and correspond respectively to the average effective optical concentration of the V-Trough alternative being analysed and to the reference set-up described. The index $\lambda$ is described in Eq. 44 and can be interpreted as the proportion of the area costs related to mirror surfaces over the area costs related to the PV absorber.

$$I_{COE(\alpha f,\alpha c)} = \left(\frac{\overline{C_{e(\alpha f,\alpha c)}}}{\overline{C_{eRef(\alpha f,\alpha c)}}}\right) * \left(\frac{LPV}{LPV + \lambda\,(LL + LR)}\right) \tag{43}$$

Where

$$\lambda = \frac{CO_s + CO_m}{CO_s + CO_{pv}} \tag{44}$$

With $CO_{pv}$ = Area cost $\left[\text{USD}/m^2\right]$ of the PV absorber, $CO_m$ = Area cost $\left[\text{USD}/m^2\right]$ of the mirrors and $CO_s$ = Area cost $\left[\text{USD}/m^2\right]$ of the supporting structures. These area cost values may vary according to the country, the year and if the implementation is either for residential or utility scale matters. However, the authors suggest the following values which may be useful as a reference.

Mirror $CO_m$ and supporting structures $CO_s$ area costs can be taken from [29] as 13.33 $\left[\text{USD}/m^2\right]$ and 62.23 $\left[\text{USD}/m^2\right]$ respectively. From [23] it was derived that the area cost of a residential PV panel of 15% efficiency is approximately 600 $\left[\text{USD}/m^2\right]$. Therefore, a suggested $\lambda$ that could be taken as a reference would be $\lambda = 0.114$.

## 6 Integrated model implementation in four different V-Trough set-ups

The most important results that can be calculated are the average effective optical concentration $\overline{C_e}$ and the cost-effectiveness index $I_{COE}$. However, one of the most important features of the model proposed is that the intermediate variables (interlinked in Fig. 1) used to calculate those indexes were selected systematically to make intuitive sense and describe the main interactions between beam radiation and the V-Trough's elements. These intermediate variables can be analysed in detail in order to understand how the geometrical input parameters affect the optical performance for every solar elevation angle throughout the range being analysed.

Four of the V-Trough set-ups used for the validation, which parameters are defined in Table 2, were selected to be explored in further detail in terms of their optical and cost-effectiveness performance. Among them, D1 and D2 were deliberately designed set-ups while S3 and S5 were defined by a random algorithm.

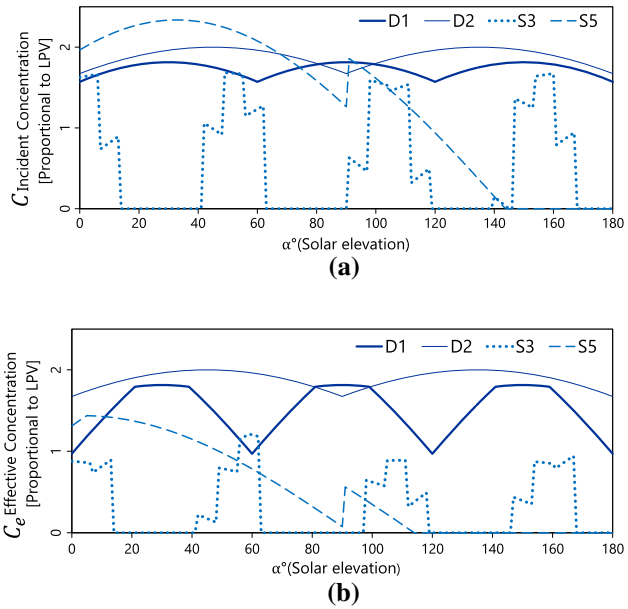


**Fig. 14** Incident concentration and Effective concentration of 4 V-Trough set-ups for the validation process

Figure 14 shows the optical performance of the four selected set-ups in terms of incident optical concentration $C$, in 14a, and Effective optical concentration $C_e$, in 14b. The figure illustrates the considerable differences that may arise within each response variable due to the optical interactions in function of the input parameters. Also, there are evident differences, within each set-up, between the curves of the $C$ and $C_e$, which emerge by taking into account the detailed optical interactions of the rays after being reflected off the mirrors. These differences underscore the need to take into account those detailed interactions, since taking $C$ as the design concentration factor may result highly misleading by assuming that every ray that reaches the device will then reach the PV absorber.

D1 and D2 achieve soft curves for the $C$ calculations. D1 has fixed mirrors with the same length as the PV absorber and has a tracking strategy such that $\beta$ starts at $\pi/3$ and moves twice in a day following a 2-step strategy. The $\beta$ tracking parameters of D1 were defined to provide the most uniform exposure to the sun with the limitation of only moving the device twice a day. On the other hand, D2 moves only once in a day in terms of its PV absorber, hence the two visible peaks, but can individually rotate its mirrors in function of the solar elevation. D2 is the only set-up that achieves the same curve with $C$ and $C_e$, since the function which controls the rotation of the mirrors ensures that every ray that reaches the mirrors is reflected towards the PV absorber and because, for the validation, the index of reflection was defined as $\rho = 1$.

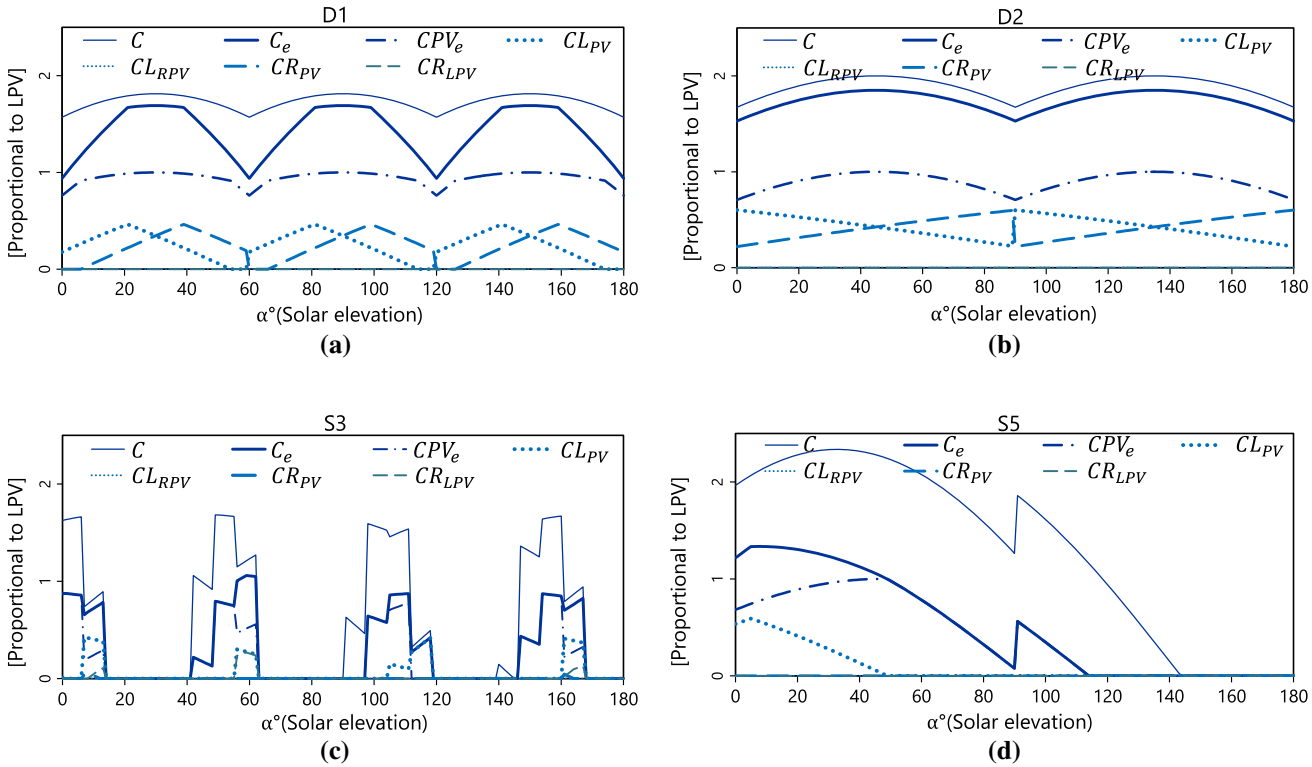


**Fig. 15** Detailed performance of set-ups D1, D2, S3 and S5

For a more realistic simulation, set-ups D1, D2, S3 and S5 were modelled again with a reflection index taken from [29] as $\rho = 0.85$, corresponding to anodized aluminium reflectors, which affects the positive impact of the mirrors. Figure 15 presents the curves for the concentration incident to the device $C$, the effective optical concentration $C_e$, and its constituent elements $CPV_e$, $CL_{PV}$, $CL_{RPV}$, $CR_{PV}$ and $CR_{LPV}$. The analysis on these curves provides much more information than just comparing set-ups by the resulting $C_e$. For instance, in Fig. 15(a) it can be inferred that the difference between $C$ and $C_e$ in D1 arises due to the sunlight that is not reflected by the mirrors and to the fact than not all the rays that reach the mirrors are reflected towards the PV absorber due to the misalignment caused by a tracking strategy of only 2 movements in a day. However, those few tracking movements do benefit considerably the optical performance, as opposed to a fixed device. The shadows casted from the mirrors only block rays from directly reaching the PV absorber during approximately the initial and final 5° of solar elevation for each of the three tracking stages.

Figure 15b can provide insight into the reasons why the curves $C$ and $C_e$ of D2 are identical, only varying proportionally to $\rho$. First, it is evident that no shadows are being casted over the PV absorber and thus, $CPV_e$ behaves the same as if the PV absorber did not have adjacent mirrors. The effect of the mirrors in D2 is symmetrical, behaves linearly in function of solar elevation and reaches the PV absorber after only one bounce, as also happens in D1.

Figure 15c shows the effects of the randomly selected tracking set-up for S3, in which $\beta$ varies so frequently and in such an angular step that it completes more than three revolutions within a day, causing the concentration curves to drop to 0 when the device is facing the floor between revolutions. It is also possible to notice that sunlight reaches the PV absorber after a second bounce, first off the right mirror and then off the left mirror, in peaks around solar elevations 10°, 60° and 165°. From Fig. 15d it can be seen that the right mirror does not provide any benefit at all, while the left one does reflect some of the rays that reach it towards the PV absorber but only up to a solar elevation of 48°. The $C_e$ of set-up S5 is mostly provided by the sunlight that directly reaches the PV absorber and this is a clear example of a detrimental implementation of V-Trough mirrors, since the negative effect of their shadows is greater than the benefit of the rays being properly focused.

Table 4 presents a summary table of the optical and cost-effectiveness performance, assessing a solar elevation range of $\alpha$ [0°, 180°] and contrasting the results with $\rho = 1$ against a more realistic modelling with $\rho = 0.85$. The sum of $LL$ and $LR$ lengths are given as proportional to the PV length.

A way to assess the inner optical performance of a V-Trough is to compare the $\overline{C}$ with the $\overline{C_e}$. With a naive $\rho = 1$,

**Table 4** Summary table for D1, D2, S3 and S5

| Set-Up ($\alpha$ [0°, 180°]) | $\overline{C}$ | $\overline{C_e}$ ($\rho = 1$) | $\overline{C_e}$ ($\rho = 0.85$) | $LL+LR$ | $I_{COE}$ ($\rho = 1$) | $I_{COE}$ ($\rho = 0.85$) |
|---|---|---|---|---|---|---|
| D1 | 1.731 | 1.516 | 1.43 | 2 | 1.950 | 1.839 |
| D2 | 1.888 | 1.888 | 1.739 | 2 | 2.428 | 2.236 |
| S3 | 0.551 | 0.303 | 0.287 | 1.6 | 0.405 | 0.383 |
| S5 | 1.328 | 0.518 | 0.502 | 2.3 | 0.648 | 0.628 |

$\overline{C_e}$ represents the 87.6%, 100%, 55% and 39% of the incident $\overline{C}$ for D1, D2, S3 and S5 respectively. Those same proportions are then reduced, with a more realistic $\rho = 0.85$, to 82.6 %, 92.1 %, 52.1 % and 37.8 % respectively. Taking into account the reflection index of the mirrors has a considerable impact over the cost-effectiveness index, and the impact increases as the contributions of the mirrors are greater, which is arguable from the fact that, when modelling with the smaller $\rho$ compared to the naive $\rho$, $I_{COE}$ was reduced by 5.7 %, 7.9 %, 5.4 % and 3.1 % respectively to D1, D2, S3 and S5. Accordingly, the $I_{COE}$ of the set-up D2 was the most affected due to the variation in $\rho$ because it is the set-up which benefits the most from the rays reflected from its mirrors.

Even though S5 has the highest mirror area, 15 % more than D1 and D2, it performs considerably worse than D1 and D2 and it even results in a $\overline{C_e}$ of 18.2 % less than the reference when $\rho = 1$ and of 20.7 % less than the reference when $\rho = 0.85$. The poor optical performance of S5, combined with a large mirror area, is reflected in its low indexes of cost-effectiveness. On the contrary, D2 presents the highest performance in cost-effectiveness, with a $I_{COE}$ of at least 21 % greater than any of the other set-ups.

## 7 Conclusions

The performed linear regression, comparing the geometrical model's predictions against corresponding measurements, is statistically equivalent to an ideal model where $Y = X$, since the significance level for the absolute difference between the regression's slope and 1 was $P$-value= 0.90324. Also supporting this conclusion, the significance level for the absolute difference between the regression's $y$ intercept and 0 was an also high $P$-value= 0.96171. Moreover, the residuals from the linear regression model did not show a systematic behaviour. Considering those facts, the proposed geometrical model concerning the effects of direct radiation is assumed to be satisfactorily corroborated.

The proposed model can support a high V-trough design flexibility, which can be argued from the up to 8 geometrical input parameters ($LPV$, $LL$, $LR$, $\beta$, $\psi L$, $\psi R$, $\rho$ and $\alpha$) that can be freely toggled by the user within the allowable ranges and may be defined as either static or in function of $\alpha$ to emulate different tracking methods. The parametric flexibility of the model were also evidenced when an unbiased random algorithm was used to define 6 V-Trough set-ups which were corroborated as correctly constructed.

The hybrid analytical-numerical nature of the model, is in accordance with the aim of an efficient model that is low in computational demands, which in turns favours the level of interactivity for a design exploration process. Even when programmed in an average personal computer, the simulations from the model are essentially in real time, with no delay perceived between the parameter inputs and the given results. Hence, it is possible for a user to rapidly iterate and analyse in detail the optical performance consequences of different set-ups. The flexible and efficient parametric nature of the model allows for a user to interactively navigate a space of V-Trough set-ups as possible solutions to a design and engineering personalised problem.

When continuous tracking is not used with a solar V-Trough device, the design concentration is not a reliable indicator for overall optical performance and consequently, the geometrical interactions between the device's elements and direct radiation should be taken into account, throughout the day, according to the given geometrical and tracking set-up. For instance, it was found that a V-Trough with two mirrors of the same length may have a design concentration of 2 incident suns, while only achieving 0.61 average effective suns throughout a day, if the device is left fixed. Moreover, even with perfect tracking, the design concentration factor can be misleading if the mirrors do not have the optimum angle and if the index of reflection is not taken into account.

As long as tracking is performed manually, or in a passive and low-cost manner, the proposed index of cost-effectiveness reasonably accounts for the relation between the gain in harvested energy and the cost for added support and mirror material. Nonetheless, since the level of tracking accuracy is not part of the cost considerations yet, a design exploration guided by the proposed index could be biased towards choosing perfect tracking, since it achieves better cost-effectiveness and average effective concentration indexes. For instance, among the set-ups that were analysed in detail, D2 achieved the highest cost-effectiveness with $I_{COE} = 2.236$. However, D2 implies that both mirrors move independently and continuously, which may probably imply

high tracking costs which are not considered in the proposed index. On the other hand, D1 could result in a more cost-effective and practical alternative, since it only implies two tracking movements throughout the day and still achieves a high $I_{COE} = 1.839$.

## 8 Further work

The presented model will be further complemented with models of diffuse radiation, temperature losses and semiconductor behaviour, enabling it to calculate the electric energy output in a more realistic and comprehensive approach. Similarly, it would be convenient to analytically take into account a possible misalignment in a third dimension, which could expand the flexibility of tracking parameters and lead to more accurate modelling. Moreover, the proposed model is planned to be implemented through optimisation and genetic algorithms to further explore its potential for V-Trough parameter definition. Even though the proposed model can already lead to useful design insights with possible industrial applications, this model is located in a wider research frame which is still under development. More research exploration and further broadening of the simulation scope are recommended in order to extend and empower its applicability in real-life design exercises.

**Acknowledgments** Special thanks to EAFIT University through the postgraduate studies grant "Undergraduate research excellence scholarship". Also, special thanks to Colciencias (Colombian Administrative Department of Science, Technology and Innovation) and, again, EAFIT University, who jointly sponsored the "Young Researchers and Innovators Program" in the 645-2014 call.

## References

1. Algarue, A., Mahmoud, S., Al-Dadah, R.: Optical performance of low concentration ratio reflective and refractive concentrators for photovoltaic applications. Energy Procedia **61**, 2375–2378 (2014)
2. Amanlou, Y., Hashjin, T.T., Ghobadian, B., Najafi, G., Mamat, R.: A comprehensive review of uniform solar illumination at low concentration photovoltaic (lcpv) systems. Renew. Sustain. Energy Rev. **60**, 1430–1441 (2016)
3. Arias-Rosales, A., Barrera-Velásquez, J., Osorio-Gómez, G., Mejía-Gutiérrez, R.: Designing a concentrating photovoltaic (cpv) system in adjunct with a silicon photovoltaic panel for a solar competition car. In: SPIE Sensing Technology+ Applications, pp. 91, 150W–91,150W. International Society for Optics and Photonics (2014)
4. Arriaga, J., Knight, J., Russell, P.S.J.: Modeling the propagation of light in photonic crystal fibers. Physica D: Nonlinear Phenomena **189**(1), 100–106 (2004)
5. Bahaidarah, H.M., Tanweer, B., Gandhidasan, P., Rehman, S.: A combined optical, thermal and electrical performance study of a v-trough pv systemexperimental and analytical investigations. Energies **8**(4), 2803–2827 (2015)
6. Bojić, M., Marjanović, N., Miletić, I., Bojić, L.: Comparison of optical performances of sea-shell trough solar concentrators. Energy Buildings **98**, 144–150 (2015)
7. Caton, P.: Design of rural photovoltaic water pumping systems and the potential of manual array tracking for a west-african village. Solar Energy **103**, 288–302 (2014)
8. Chen, J., Li, X., Nilson, T., Strahler, A.: Recent advances in geometrical optical modelling and its applications. Remote Sens. Rev. **18**(2–4), 227–262 (2000)
9. Famoso, F., Lanzafame, R., Maenza, S., Scandura, P.F.: Performance comparison between low concentration photovoltaic and fixed angle pv systems. Energy Procedia **81**, 516–525 (2015)
10. Fatih-Orhan, M., Sharaf, O.Z.: Concentrated photovoltaic thermal (cpvt) solar collector systems: Part ii–implemented systems, performance assessment, and future directions (2015)
11. Fischer, X., Coutellier, D.: Research in interactive design: proceedings of virtual concept 2005. Springer, Paris, France (2006)
12. Fischer, X., Nadeau, J.-P.: Interactive design: then and now. In: Research in Interactive Design Vol. 3, pp. 1–5. Springer, Paris, France (2011)
13. Fraidenraich, N.: Analytic solutions for the optical properties of v-trough concentrators. Applied optics **31**(1), 131–139 (1992)
14. Fraidenraich, N.: Design procedure of v-trough cavities for photovoltaic systems. Progr. Photovoltaics Res. Appl. **6**(1), 43–54 (1998)
15. Gotelli, N., Ellison, A.: A Primer of Ecological Statistics. Macmillan Education (2013). https://books.google.com.co/books?id=zTbjMQEACAAJ
16. Grynberg, G., Aspect, A., Fabre, C.: Introduction to quantum optics: from the semi-classical approach to quantized light. Cambridge University Press, Cambridge (2010)
17. Gupta, B.P., Anderson, J.V.: Solar detoxification of hazardous waste-an overview of the us department of energy program. Solar Energy Mater. **24**(1), 40–61 (1991)
18. Hermenean, I., Visa, I., Diaconescu, D.: On the geometric modelling of a concentrating pv-mirror system. Bull. Transilvania Univ. Braşov **2**, 51 (2009)
19. Kelly, N.A., Gibson, T.L.: Improved photovoltaic energy output for cloudy conditions with a solar tracking system. Solar Energy **83**(11), 2092–2102 (2009)
20. Kostić, L.T., Pavlović, T., Pavlović, Z.: Optimal design of orientation of pv/t collector with reflectors. Appl. Energy **87**(10), 3023–3029 (2010)
21. Lins, I.D., Droguett, E.L., das Chagas Moura, M., Zio, E., Jacinto, C.M.: Computing confidence and prediction intervals of industrial equipment degradation by bootstrapped support vector regression. Reliabil. Eng. Syst. Safety **137**, 120–128 (2015)
22. Lo, C.K., Lim, Y.S., Rahman, F.A.: New integrated simulation tool for the optimum design of bifacial solar panel with reflectors on a specific site. Renewable Energy **81**, 293–307 (2015)
23. MIT: The Future of Solar Energy-AN INTERDISCIPLINARY MIT STUDY. MIT, Cambridge (2015)
24. O'Kane, S.E., Sarma, J., Allsopp, D.W.: A quasi-analytic modal expansion technique for modeling light emission from nanorod leds. Quant. Elect. IEEE J. **50**(9), 774–781 (2014)
25. Pedrotti, L.S.: Module 1.3: basic geometrical optics. In: Roychoudhuri, C. (ed.) Fundamentals-of-photonics-modules. SPIE Press, USA (2012)
26. Penttilä, A., Lumme, K.: The effect of the properties of porous media on light scattering. J. Quantitative Spectrosc. Radiat. Transfer **110**(18), 1993–2001 (2009)
27. Reis, F., Brito, M., Corregidor, V., Wemans, J., Sorasio, G.: Modeling the performance of low concentration photovoltaic systems. Solar Energy Mater. Solar Cells **94**(7), 1222–1226 (2010)
28. Reis, H.T., Judd, C.M.: Handbook of research methods in social and personality psychology. Cambridge University Press, Cambridge (2000)

29. Sangani, C., Solanki, C.: Experimental evaluation of v-trough (2 suns) pv concentrator system using commercial pv modules. Solar Energy Mater. Solar Cells **91**(6), 453–459 (2007)
30. Savio, G., Concheri, G., Meneghello, R.: Progressive lens design by discrete shape modelling techniques. Int. J. Interactive Des. Manuf. (IJIDeM) **7**(3), 135–146 (2013)
31. Shanks, K., Senthilarasu, S., Mallick, T.K.: Optics for concentrating photovoltaics: trends, limits and opportunities for materials and design. Renewable Sustainable Energy Rev. **60**, 394–407 (2016)
32. Sheng, Y., Shi, Y., Wang, L., Narasimhan, S.G.: A practical analytic model for the radiosity of translucent scenes. In: Proceedings of the ACM SIGGRAPH Symposium on Interactive 3D Graphics and Games, pp. 63–70. The Association for Computing Machinery, Inc, New York, USA (2013)
33. Taylor, A.E.F.: Illumination fundamentals. Rensselaer Polytechnic Institute, Pasadena, USA (2000)
34. Tina, G., Scandura, P.: Case study of a grid connected with a battery photovoltaic system: V-trough concentration vs. single-axis tracking. Energy Conversion Manag. **64**, 569–578 (2012)
35. Velzel, C.: A course in lens design, vol. 183. Springer, Netherlands (2014)
36. Vergnano, A., Berselli, G., Pellicciari, M.: Parametric virtual concepts in the early design of mechanical systems: a case study application. Int. J. Interactive Des. Manuf. (IJIDeM), 1–10 (2015). doi:10.1007/s12008-015-0295-y